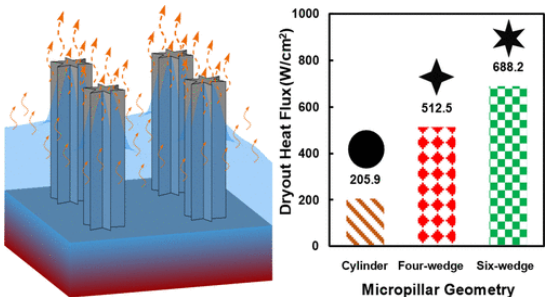


Sl. No.	<p style="text-align: center;"><b>IIT Ropar</b>  <b>List of Recent Publications with Abstract</b>  <b>Coverage: May, 2023</b></p>
1.	<p><a href="#">ACPC: Covert channel attack on last level cache using dynamic cache partitioning</a>  J Kaur, S Das - 24th International Symposium on Quality Electronic Design (ISQED): Conference Proceeding, 2023</p> <p><b>Abstract:</b> The Last Level Cache (LLC) of modern multicore processors is normally shared between different cores and applications. Dynamic cache partitioning is applied to the LLC for fairly distributing the LLC space among the applications. Recently, Covert Channel Attacks (CCA) becomes a major security issue for modern multicore systems. In CCA, two malicious applications: spy and Trojan, run in two different cores. Trojan normally runs in a secure core and knows some secret information. Through CCA, Trojan communicates this information to the spy. A well-known technique to perform such an attack is Prime Probe (P+P). It performs the attack by using the shared behavior of LLC space. Cache partitioning is considered a defense against such CCA. Partitioning makes the applications isolated in the LLC and they cannot evict each other block from the LLC. Hence, the existing P+P based attacks are not possible while dynamic partitioning is applied to LLC. However, in this work, we have proposed a modified CCA (based on P+P) which can establish a covert channel on top of the dynamic cache partitioning technique applied to LLC. Such kinds of attacks must need to be handled carefully in modern processors. A possible defense mechanism for the new attack is also discussed in this paper.</p>
2.	<p><a href="#">Age-mediated gut microbiota dysbiosis promotes the loss of dendritic cells tolerance</a>  H Bashir, S Singh, RP Singh, JN Agrewala... - Aging Cell, 2023</p> <p><b>Abstract:</b> The old age-related loss of immune tolerance inflicts a person with a wide range of autoimmune and inflammatory diseases. Dendritic cells (DCs) are the sentinels of the immune system that maintain immune tolerance through cytokines and regulatory T-cells generation. Aging disturbs the microbial composition of the gut, causing immune system dysregulation. However, the <i>vis-à-vis</i> role of gut dysbiosis on DCs tolerance remains highly elusive. Consequently, we studied the influence of aging on gut dysbiosis and its impact on the loss of DC tolerance. We show that DCs generated from either the aged (DC<sup>Old</sup>) or gut-dysbiotic young (DC<sup>Dysbiotic</sup>) but not young (DC<sup>Young</sup>) mice exhibited loss of tolerance, as evidenced by their failure to optimally induce the generation of Tregs and control the overactivation of CD4<sup>+</sup> T cells. The mechanism deciphered for the loss of DC<sup>Old</sup> and DC<sup>Dysbiotic</sup> tolerance was chiefly through the overactivation of NF-κB, impaired frequency of Tregs, upregulation in the level of pro-inflammatory molecules (IL-6, IL-1β, TNF-α, IL-12, IFN-γ), and decline in the anti-inflammatory moieties (IL-10, TGF-β, IL-4, IDO, arginase, NO, IRF-4, IRF-8, PDL1, BTLA4, ALDH2). Importantly, a significant decline in the frequency of the <i>Lactobacillus</i> genus was noticed in the gut. Replenishing the gut of old mice with the <i>Lactobacillus plantarum</i> reinvigorated the tolerogenic function of DCs through the rewiring of inflammatory and metabolic pathways. Thus, for the first time, we demonstrate the impact of age-related gut dysbiosis on the loss of DC tolerance. This finding may open avenues for therapeutic intervention for treating age-associated disorders with the <i>Lactobacillus plantarum</i>.</p>
3.	<p><a href="#">An experimentally informed computational framework for investigating the role of surface roughness on high cycle fatigue life of lpb in 718</a>  S Kumar, DK Mahajan, J Bouhattate, D Srinivasan - Transactions of the Indian National Academy of Engineering, 2023</p> <p><b>Abstract:</b> The present study attempts to model the surface roughness of additive manufactured (AM) Inconel 718 (IN718) via the laser powder bed fusion (LPBF) process. A MATLAB code is</p>

	<p>developed to generate a rough surface, to match the experimental measurements of surface roughness after printing, grit blasting, and fine polishing (6, 2, and 0.5 <math>\mu\text{m } R_a</math>, respectively). Stress analysis carried out using ABAQUS and FE-Safe has been used to calculate and predict the fatigue life as a function of the roughness. LPBF IN718 samples are characterized for microstructure and mechanical properties to incorporate the room temperature material properties in simulation in the as printed and heat-treated condition. The surface microstructural features in the as-printed condition showed un-melted particles, contributing to high roughness values. Simulation can correlate the fatigue life to be inversely proportional to the surface roughness and establish that the stress gradient along the depth of a rough surface plays a crucial role in crack propagation. A sensitivity analysis has been carried out on the role of surface roughness to enable predicting the fatigue life in part geometries with inaccessible locations.</p>
4.	<p><a href="#">Beta Elemene induces cytotoxic effects in FLT3 ITD-mutated acute myeloid leukemia by modulating apoptosis</a>  A. Alafnan, R. Dogan, O. Bender, I. Celik, A. Mollica, J.A. Malik - European Review for Medical &amp; Pharmacological Sciences, 2023</p> <p><b>Abstract:</b>  OBJECTIVE: <math>\beta</math>-Elemene, a sesquiterpene with a broad anti-cancer spectrum, is particularly effective against drug-resistant and complex tumors. It can also be efficient against FLT3-expressed acute myeloid leukemia. This research aims to determine whether <math>\beta</math>-Elemene has cytotoxic effects on FLT3 ITD-mutated AML cells.  MATERIALS AND METHODS: Cytotoxicity, cell morphology, mRNA analysis with apoptotic markers, and analysis of 43 distinct protein markers related to cell death, survival, and resistance were all performed to elucidate its mechanism. Additionally, in order to understand how <math>\beta</math>-Elemene and FLT3 interact, molecular docking, molecular dynamics simulations, and computational ADME investigations were performed.  RESULTS: <math>\beta</math>-Elemene exhibited cytotoxic activity against FLT3-mutated MV4-11 and FLT3 wild-type THP-1 cells, with an IC<sub>50</sub> of around 25 <math>\mu\text{g/ml}</math>. The molecular studies revealed that <math>\beta</math>-Elemene inhibited cell proliferation by inducing p53, and the involvement of p21, p27, HTRA, and HSPs were also demonstrated. The interactive inhibition in proliferation was confirmed via molecular docking and dynamics analyses. <math>\beta</math>-Elemene occupied the FLT3 enzymatic pocket with good stability at the FLT3 active site.  CONCLUSIONS: We concluded from our observations that <math>\beta</math>-Elemene causes cell death in ITD mutant AML cells, together with the effects of stress factors and inhibiting cell division.</p>
5.	<p><a href="#">Biomimetic micropillar wick for enhanced thin-film evaporation</a>  Anand S, CS Sharma – Langmuir, 2023</p> <p><b>Abstract:</b> Sustainable liquid cooling solutions are recognized as the future of thermal management in the chip industry. Among them, phase change heat transfer devices such as heat pipes and vapor chambers have shown tremendous potential. These devices rely on the physics of capillary-driven thin-film evaporation, which is inherently coupled with the design and optimization of the evaporator wicks used in these devices. Here, we introduce a biomimetic evaporator wick design inspired by the peristome of the <i>Nepenthes alata</i> that can achieve significantly enhanced evaporative cooling. It consists of an array of micropillars with multiple wedges along the sidewall of each micropillar. The efficacy of the wedged micropillar is evaluated based on a validated numerical model on the metrics of dryout heat flux and effective heat transfer coefficient. The wedge angle is chosen such that wedged micropillars cause liquid filaments to rise along the micropillar vertical walls. This results in a significant increase in thin-film area for evaporation. Additionally, the large mean curvature of the liquid meniscus produces strong capillary pumping pressure and simultaneously, the wedges increase the overall permeability of the wick. Consequently, our model predicts that the wedged micropillar wick can attain ~234% enhancement of dryout heat flux compared to a conventional cylindrical</p>

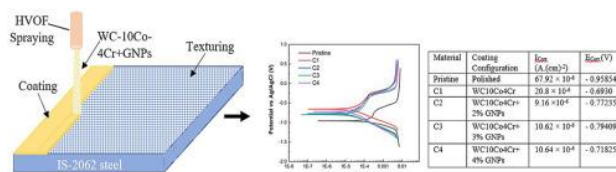
	<p>micropillar wick of similar geometrical dimensions. Moreover, the wedged micropillars can also attain a higher effective heat transfer coefficient under dryout conditions, thus outperforming the cylindrical micropillar in terms of heat transfer efficiency. Our study provides insight into the design and capability of the biomimetic wedged micropillars as an efficient evaporator wick for various thin-film evaporation applications.</p>  <p>The figure shows a 3D schematic of micropillars on a substrate with heat being applied. To the right is a bar chart titled 'Dryout Heat Flux (W/cm²)' vs 'Micropillar Geometry'. The chart compares three geometries: Cylinder (205.9), Four-wedge (512.5), and Six-wedge (688.2). The Six-wedge geometry shows the highest performance, indicated by a star symbol.</p> <table border="1"> <thead> <tr> <th>Micropillar Geometry</th> <th>Dryout Heat Flux (W/cm²)</th> </tr> </thead> <tbody> <tr> <td>Cylinder</td> <td>205.9</td> </tr> <tr> <td>Four-wedge</td> <td>512.5</td> </tr> <tr> <td>Six-wedge</td> <td>688.2</td> </tr> </tbody> </table>	Micropillar Geometry	Dryout Heat Flux (W/cm²)	Cylinder	205.9	Four-wedge	512.5	Six-wedge	688.2
Micropillar Geometry	Dryout Heat Flux (W/cm²)								
Cylinder	205.9								
Four-wedge	512.5								
Six-wedge	688.2								
6.	<p><a href="#">Candle soot nanoparticle embedded nanofibrous membrane for separation of miscible and immiscible oil/water mixtures</a>  K Thota, K Donthula, C Shekhar, R Vooradi, M Sabathy - Polymer Composites, 2023</p> <p><b>Abstract:</b> Candle soot (CS) nanoparticles exhibit excellent superhydrophobic and superoleophilic properties, making them an ideal absorbent for separating oil and oil/water mixtures. Although their cost-effectiveness is attractive, the challenges associated with recovering soot nanoparticles after oil absorption and producing secondary pollutants have limited their attention. Our study demonstrates the synthesis of CS nanoparticles embedded polystyrene (PS) nanofibrous membranes with excellent stability, surface-to-volume ratios, and flexibility. CS-incorporated composite membrane with a rough surface showed a water contact angle (WCA) of <math>156^\circ \pm 1.5^\circ</math>, about 20% higher than the smooth pristine PS membrane. The CS-based composite membrane also demonstrated improved performance as an absorbent, owing to its hydrophobic characteristics linked with surface roughness when employed for separating oil from oil/water mixtures. Furthermore, when exposed to four different oils, the CS-based membrane displayed a higher absorption capacity (up to <math>\approx 120</math> g oil/g membrane) than the pristine membrane. Using a gravity-assisted continuous oil/water separation setup, we measured the oil permeate flux using nanofiber mats as a membrane. Compared to the original membrane, the modified membrane showed enhanced oil permeate flux of <math>\sim 2873 \pm 122</math> L m<sup>-2</sup> h<sup>-1</sup> and separation efficiency of over 99%.</p>								
7.	<p><a href="#">Chitosan–poly(vinyl alcohol)–ionic liquid-grafted hydrogel for treating wastewater</a>  A Singh, N Singh, N Kaur, DO Jang - New Journal of Chemistry, 2023</p> <p><b>Abstract:</b> A chitosan–poly(vinyl alcohol)–ionic liquid-grafted hydrogel was prepared for water purification. The hydrogel was characterized using various techniques, including nuclear magnetic resonance spectroscopy, X-ray photoelectron spectroscopy, infrared spectroscopy, powder X-ray diffraction, scanning electron microscopy, and energy-dispersive spectroscopy. The swelling properties of the hydrogels were optimized by varying the solvent, pH, time, and temperature. The maximum swelling of the hydrogel was 330%. The hydrogel absorbed dye, nitrite, and Pb<sup>2+</sup>, with removal rates of up to 97% for dye and 88% for Pb<sup>2+</sup>. The hydrogel could effectively recover oil from an oil–water mixture, where the removal mechanism was predominantly attributed to electrostatic interactions between the cationic hydrogel and the dye, Pb<sup>2+</sup>, and nitrite anions. The hydrogel was biodegradable, making it environmentally friendly.</p>								
8.	<p><a href="#">Choline based deep eutectic solvent for denitrogenation of liquid fuel: A molecular dynamics study</a>  K Kumar, A Bharti, A Kumar, SK Ghosh, A Kumar - Journal of Molecular Liquids, 2023</p>								

	<p><b>Abstract:</b> Deep eutectic solvents, a new genre of green solvent, easy to synthesize, low volatility and non-toxic in nature, emerged as an efficient extractant for denitrogenation. We have performed a molecular dynamics simulation study to investigate the role of glyceline as an extractant for removal of nitrogen impurities namely indole, pyrrole, pyridine, and quinoline from a model liquid fuel. <math>\Delta G_{\text{transfer}}</math> was evaluated to capture the thermodynamic feasibility of the transfer of nitrogen impurities from the fuel to the glyceline phase. Negative value of <math>\Delta G_{\text{transfer}}</math> was obtained for the nitrogen impurities, and the partition coefficient in the following order: indole &gt; pyrrole &gt; quinoline &gt; pyridine. The simulation revealed that the chloride-ion possesses strong interaction with indole and pyrrole while glycerol favors quinoline and pyridine. The fuel phase was observed to be free from impurities while glyceline phase contained impurities, which was confirmed by the negative and positive values of <math>\Delta G_{\text{transfer}}</math> and partition coefficient respectively. The self-diffusion coefficient for indole was observed to be the lowest while pyridine possesses the highest value, which was found to be in agreement with the observations from radial and spatial distribution functions. Further, this understanding at the atomic level for liquid-liquid extraction will help in developing potential solvents for denitrogenation of liquid fuel.</p>
9.	<p><a href="#"><u>Coalescence of au nanoparticles in silica aerogel under electron beam irradiation</u></a>  H Sammi, M Mohanta, B Sharma, N Sardana - Current Nanoscience, 2023</p> <p><b>Abstract:</b>  Background: The coalescence of Au nanoparticles embedded in the silica gel matrix was observed by E-beam irradiation in a transmission electron microscope.  Methods: It was examined that interparticle spacing between nanoparticles was reduced after incorporation into the matrix and particles came close to each other. TEM studies have shown that during E-beam irradiation ~13 nm Au nanoparticles contacted with each other along with the shrinkage of the silica aerogel or as well as the removal of surfactant layer, and transformed into different shapes of particles such as dumbbell and chain-like particles as per the interparticle gap.  Results: This nanoparticle-aerogel matrix has the potential for applications in sensing, nonlinear optics, and catalysis.  Conclusion: This work enhances the understanding of the role of silica aerogel and E-beam irradiation in directing the coalescence of nanoparticles.</p>
10.	<p><a href="#"><u>Comparative corrosion behaviour of cold sprayed titanium/hydroxyapatite and titanium/baghdadite composite coatings in simulated body fluid environment</u></a>  A Kumar, T Chand, R Kant, H Singh – ITSC: Conference Proceedings, 2023</p> <p><b>Abstract:</b> Bioceramics deposition on medical devices is a widespread area of research for biomedical industries since such deposits can induce excellent chemical and biological properties to the devices. Thermal spraying has been a popular choice for developing coatings to enhance the mechanical, chemical, and biological responses of medical devices. However, the high heat involved during the thermal spraying of bioceramics limits their functionality. In this context, low processing temperature in cold spraying is believed to protect the bioceramics from degradation. However, depositing bioceramics using cold spray and achieving good mechanical properties are still challenging tasks because of their poor ductility. Therefore, bio metal matrix composites with reinforced bioceramics produced using cold spray are expected to give good mechanical, chemical, and biological properties. The present work presents deposition and microstructural characterization of titanium/hydroxyapatite (Ti/HA) and titanium/baghdadite (Ti/BAG) composite coatings by cold spraying. Furthermore, the comparative corrosion response of these coatings under a simulated body fluid environment is reported. The effect of laser remelting on microstructure and corrosion behavior is also discussed.</p>
11.	<p><a href="#"><u>Corrosion behaviour of laser textured and WCCoCr+GNPs coated IS-2062 steel</u></a>  V Kumar, NK Singh, R Verma, DK Mahajan, VS Sharma - Diamond and Related Materials, 2023</p>



**Abstract:** WC10Co4Cr and WC10Co4Cr + (2 %, 3 %, 4 %) graphene nanoplatelets (GNPs) coatings were applied on laser-textured (circular shape: 100  $\mu\text{m}$  in diameter and 200  $\mu\text{m}$  in pitch) IS-2062 steel using the HVOF technique. The surface morphology of coated and uncoated surfaces was investigated using SEM, XRD, and EDS prior and after electrochemical corrosion tests in 3.5 % NaCl solution at room temperature. The results show that the coating binder (Co and Cr alloys) breaks down in NaCl solution, leading to localized pitting corrosion on the surface. The addition of GNPs to WC10Co4Cr coating powder improved the surface's corrosion resistance and reduced the emergence of localized pits. The WC10Co4Cr + 2%GNPs-coated substrate exhibited the lowest corrosion rate of (0.078361 mm/year) compared to other coatings and pristine substrate with the highest corrosion rate of (0.70679 mm/year).

#### Graphical Abstract:



#### Dynamics of cobalt oxide nanoparticles in the activation of reactive oxygen species-induced inflammation and immunomodulation

S Chattopadhyay, S Roy - Handbook of Oxidative Stress in Cancer: Mechanistic Aspects, 2023

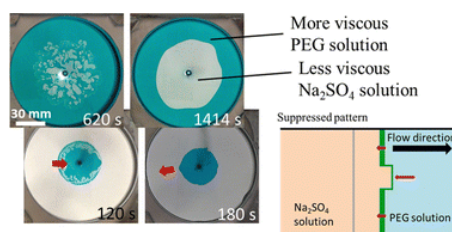
**Abstract:** The progress of nanoparticles (NPs) in cancer therapy introduces a better efficacy and lower toxicity for treatment. The cobalt oxide nanoparticles (CoO NPs) were prepared by the calcination method. The nano states of the particles were confirmed by different available physio-chemical estimations. The CoO NPs induce toxicity by leaching of  $\text{Co}^{2+}$  ions that strongly trigger the generation of reactive oxygen species (ROS) and activate the caspase cascade followed by necrosis on three different cancer cell lines (jurkat, KG1-A, and K562 cells) as well as the normal counterparts. The toxicity of the CoO NPs was minimized by using different surface modifying agents, such as phosphonomethyl iminodiacetic acid (PMIDA) and chitosan (CS). Surface modifications significantly reduced the  $\text{Co}^{2+}$  ion release into the media and reduced the toxicity of surface-modified CoO NPs to normal cells, whereas in the cancer microenvironment, modified NPs liberate  $\text{Co}^{2+}$  ions which induced anticancer activity by activating ROS in association with TNF- $\alpha$  and p38 MAPK, followed by activation of caspase cascade in both in vitro and in vivo systems. Among the two, the PMIDA-CoO NPs showed better activity at low concentrations. Independent treatment of PMIDA-CoO NPs could trigger the release of interferon gamma (IFN- $\gamma$ ), tumor necrosis factor alpha (TNF- $\alpha$ ), interleukin 12 (IL-12), and decrease the production of interleukin 10 (IL-10) from lymphocytes and macrophage and produced a pro-inflammatory response.

The surface pendant -COOH group of PMIDA-CoO NPs showed an excellent binding affinity with cancer cell lysate (CL), used as an antigen. The protein antigen conjugated PMIDA-CoO NPs stimulated the macrophage and produced a strong anticancer immune response. The antitumor activity of the antigen conjugated nanoparticle (CL-PMIDA-CoO NPs) pulsed macrophages were tested on a human oral carcinoma cell line (KB) in vitro. The modified CL-PMIDA-CoO NPs upregulated IFN- $\gamma$ , TNF- $\alpha$ , and induced an anticancer immune response by activating macrophages. The use of nuclear factor kappa beta (NF- $\kappa\beta$ ), TNF- $\alpha$ , and Cyclooxygenase-2 (COX-2) inhibitors confirmed the ability of the CL-PMIDA-CoO nano-complex to induce TNF- $\alpha$  associated immunostimulation. CL-PMIDA-CoO nanoparticles efficiently increased the  $\text{CD4}^+$  population. In vivo immunization of antigen conjugated PMIDA-

	<p>CoO NPs induced an antigen-specific Immunoglobulin G (IgG) response and amplified the antibody dependent cellular cytotoxic (ADCC) effect. The cell lysate conjugated PMIDA-CoO NPs successfully activated the antigen presenting cells (APCs) as evinced by the elevated level of IFN-<math>\gamma</math> and TNF-<math>\alpha</math> in serum. Additionally, the nanoconjugate can re-modulate the immune-suppressive tumor-associated macrophages towards pro-tumor macrophage by activating nicotinamide adenine dinucleotide phosphate oxidase (NADPH oxidase)-ROS-p38 MAPK pathway. Thus, our findings provide insights into the use of PMIDA-CoO NPs as antigen delivery vehicles.</p>
13.	<p><a href="#">Effect of foundation flexibility on seismic performance of reinforced concrete shear wall buildings</a>  KKK Reddy, P Haladar - AIP Conference Proceedings, 2023</p> <p><b>Abstract:</b> Rapid urbanization and land scarcity lead to the absolute necessity of high-rise building construction on any available land irrespective of soil type. Dynamic properties of stiff building such as Reinforced Concrete (RC) frame with shear walls resting on soft soil may greatly be influenced by Soil-Structure Interaction (SSI) and alter the seismic performance of such building. In order to assess the realistic behaviour of reinforced concrete shear wall buildings under the combined action of gravity and lateral loading, an effort has been made to assess explicit implication of SSI by comparing seismic performance of a set of mid-rise and high-rise RC shear wall buildings considering SSI with their fixed base counterpart. Nonlinear static analysis has been performed to evaluate seismic performance through strength, stiffness, and ductility of the considered set of buildings with and without SSI. It is observed that the effect of SSI is predominant as the height of the building increases. Lateral load-carrying capacity of high-rise buildings with foundation flexibility differs significantly and alters the seismic performance of the building than that of fixed based counterpart asserting absolute necessity for inclusion of foundation flexibility while analysing and designing high-rise buildings in order to predict realistic behaviour of such buildings.</p>
14.	<p><a href="#">Effect of thermal ageing on space charge dynamics in ldpe</a>  S Dhayalan, CC Reddy - IEEE Transactions on Dielectrics and Electrical Insulation, 2023</p> <p><b>Abstract:</b> Understanding space charge phenomenon in polyethylene under long-term thermal stress is essential and is of huge practical importance. In this paper, low density polyethylene (LDPE) sheet samples are thermally aged for upto 256 days and space charge dynamics are investigated at low and high electric fields experimentally. For highly aged samples, the space charge is measured in the vicinity of breakdown. A clear difference in trend of packet-like charge movement is observed in the highly aged samples when compared to packet charge of fresh samples reported until now. Interesting insights on the injection and movement of charges through the bulk, mean accumulated charge density, field enhancement factor as well as the shift of space charge regimes with ageing are presented, which were apparently not given adequate attention in the literature so far. The results are believed to be useful for HVDC insulation designers and utilities.</p>
15.	<p><a href="#">Efficient placement and migration policies for an STT-RAM based hybrid L1 cache for intermittently powered systems</a>  SJ Badri, M Saini, N Goel - Design Automation for Embedded Systems, 2023</p> <p><b>Abstract:</b> The number of battery-powered devices is rapidly increasing due to the widespread use of IoT-enabled nodes in various fields. Energy harvesters, which help to power embedded devices, are a feasible alternative to replacing battery-powered devices. In a capacitor, the energy harvester stores enough energy to power up the embedded device and compute the task. This type of computation is referred to as intermittent computing. Energy harvesters are unable to supply continuous power to embedded devices. All registers and cache in conventional processors are volatile. We require a Non-Volatile Memory (NVM)-based Non-Volatile</p>

	<p>Processor (NVP) that can store registers and cache contents during a power failure. NVM-based caches reduce system performance and consume more energy than SRAM-based caches. This paper proposes Efficient Placement and Migration policies for hybrid cache architecture that uses SRAM and STT-RAM at the first level cache. The proposed architecture includes cache block placement and migration policies to reduce the number of writes to STT-RAM. During a power failure, the backup strategy identifies and migrates the critical blocks from SRAM to STT-RAM. When compared to the baseline architecture, the proposed architecture reduces STT-RAM writes from 63.35% to 35.93%, resulting in a 32.85% performance gain and a 23.42% reduction in energy consumption. Our backup strategy reduces backup time by 34.46% when compared to the baseline.</p>
16.	<p><a href="#">Ergodic secrecy capacity of backscatter communication based automatic toll collection systems</a> HK Sharma, B Kumbhani - Sādhanā, 2023</p> <p><b>Abstract:</b> Automatic toll collection systems have been known to operate with a backscatter mechanism. Such systems are highly prone to eavesdropping despite the security measures implemented, as the data can be stored and processed later for the transaction. In this paper, we analyse the probability that secrecy is compromised in the automatic toll collection systems using the physical layer security principles. We perform simulations to corroborate the analytical results in the proposed fading channel environment. The results are obtained for different distances between the tag and the reader and that between the tag and the eavesdropper. The analytical and simulation results are found to be in close agreement.</p>
17.	<p><a href="#">Evaluation of flow boiling heat transfer in horizontal circular trapezoidal-shaped microfin tube</a> S Deb, M Das, DC Das, S Pal, R Das, AK Das - Heat and Mass Transfer, 2023</p> <p><b>Abstract:</b> Experimental investigations were conducted to analyze the evaporation heat transfer of R407c inside a horizontal microfin (trapezoidal-shaped) Cu-tube. The experiments were performed in equipment specifically designed and fabricated for phase change analysis, with a test section consisting of a 1m long Cu-tube with an outer diameter of 9.52 mm and a recirculating water heating system. The following test parameters were used: a heat flux of 5-85 kW.m<sup>-2</sup>, mass flux of 20-350 kg.m<sup>-2</sup>.s<sup>-1</sup>, vapor quality range of 0.03-0.667, and saturation temperature of 283.15-313.15 K. The novel aspect of this study is the newly designed microfin tube with helix and apex angles of 22° and 48°, fin height of 0.22 mm, and a total of 60 fins. Following experimental analysis, flow boiling heat transfer coefficients rise with mass flux, vapor quality, lower saturation temperature, hydraulic diameter, and heat flux. The experimental outcomes were also compared with established correlations. The error range for the experimental data was found to be within ±25%±25%, which shows that the data are accurate to a high level of 95%. Besides that, correlations of evaporation heat transfer through a 9.52 mm horizontal round microfin tube were established by using the interpolation technique in LINGO software to anticipate the internal evaporator heat transfer coefficient as a consequence of saturation temperature. At saturation temperatures of 283.15 K and 293.15 K, the new correlation can predict most of the previous experimental results within ±20%±20% the error margin.</p>
18.	<p><a href="#">Experimental demonstration of the suppression of viscous fingering in a partially miscible system</a> K Iwasaki, Y Nagatsu, T Ban...M Mishra... - Physical Chemistry Chemical Physics, 2023</p> <p><b>Abstract:</b> Phase separation is ubiquitous in nature and technology. So far, the focus has primarily been on phase separation occurring in the bulk phase. Recently, phase separation taking place in interfacial areas has attracted more attention – in particular, a combination of interfacial phase separation and hydrodynamics. Studies on this combination have been conducted intensively in this past decade; however, the detailed dynamics remain unclear. Here, we perform fluid displacement experiments, where a less viscous solution displaces a more viscous one in a radially confined geometry and phase separation occurs at the interfacial region.</p>

We demonstrate that a finger-like pattern, due to the viscosity contrast during the displacement, can be suppressed by the phase separation. We also claim that the direction of a body force, the so-called Korteweg force, which appears during the phase separation and induces convection, determines whether the fingering pattern is suppressed or changed to a droplet pattern. The change of the fingering pattern to the droplet pattern is enhanced by the Korteweg force directed from the less viscous solution to the more viscous one, whereas the fingering is suppressed by the force directed in the opposite direction. These findings will contribute directly to the higher efficiency of processes such as enhanced oil recovery and CO<sub>2</sub> sequestration, where interfacial phase separation is considered to occur during the flow.



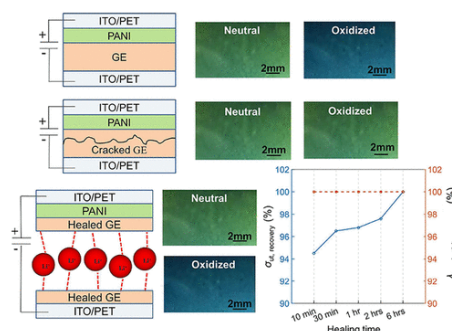
### [Exploiting self-healing characteristics of poly\(methyl methacrylate\) in gel electrolyte for application in electrochromic devices](#)

V Agrawal, E Singla, PK Agnihotri - ACS Applied Engineering Materials, 2023

19.

**Abstract:** Self-healing characteristics in a gel electrolyte (GE) are desirable to improve the optical performance and service life of an electrochromic device (ECD). By exploiting the healing properties of poly(methyl methacrylate) (PMMA), the fabrication and characterization of GE with self-healing capabilities are reported here. Comparative mechanical and electrochemical analyses of the original and healed GE samples are performed to determine the optimum PMMA concentration and healing time. Experimental results show that the GE with 15 wt % of PMMA (GE15) recovers 98% of its mechanical strength within 10 min of healing time. The ionic conductivities of the healed samples are found to be the same as that of the original sample at all PMMA concentrations and healing times. It is observed that the healing time, viscosity, number of uncoiling polymer chains, and mobility of Li<sup>+</sup> ions critically influence the healing efficiency of a GE. Color contrast analyses of ECDs fabricated with original and healed GEs are performed to demonstrate the applicability of self-healable GEs. It is recorded that for longer healing times the color performances of self-healed ECDs approach that of the original ECD. The findings of the present study will help to develop repair strategies for ECDs and improve their service life.

#### Graphical Abstract:



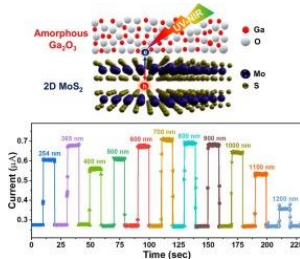
### [Fabrication and characterization of liquid phase exfoliated mos2 nanosheet for gas sensing application](#)

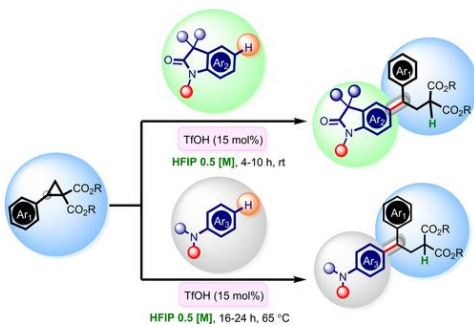
R Gond, A Rawat...B Rawat - IEEE Applied Sensing Conference, 2023

20.

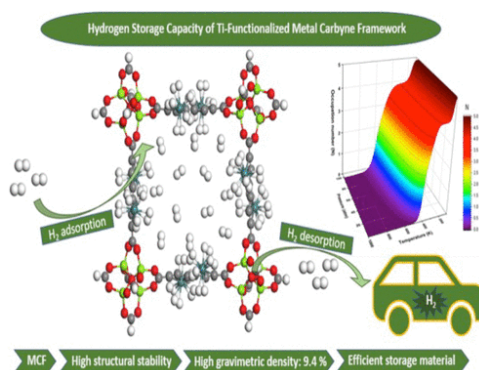


	<p><b>Abstract:</b> Due to its excellent chemical and electronic properties, two-dimensional MoS<sub>2</sub> has emerged as a viable candidate for developing near-room temperature gas sensors with high selectivity and sensitivity. However, most of the reported sensors have synthesized the MoS<sub>2</sub> sheet using chemical vapor phase deposition or hydrothermal method, which makes them unsuitable for large-scale sensor printing process. In this regard, we fabricate and characterize the n-type and p-type MoS<sub>2</sub> based electrochemical sensors using the liquid phase exfoliation method for a superior NO<sub>2</sub> sensor at near room temperature. Liquid phase exfoliation of MoS<sub>2</sub> is one of the most simple and cost-effective method that could be more suitable for large-scale printing process. The synthesized MoS<sub>2</sub> nanosheets were characterized by Zeta potential measurement, scanning electron microscopy (SEM), and Raman spectroscopy. The results show that the p-type MoS<sub>2</sub> nanosheet offers a high response and good selectivity to NO<sub>2</sub> gas at room temperature.</p>
21.	<p><a href="#">Fabrication of FRET based nano sensor from biomass-derived fluorescent carbon quantum dots and naphthalimide for ratiometric detection of nitric oxide: To examine nitrite levels in meat samples</a>  A Singh, G Singh, N Kaur, N Singh - <i>Analytica Chimica Acta</i>, 2023</p> <p><b>Abstract:</b> Nitric oxide (NO) is a ubiquitous, gaseous, free radical signaling molecule which plays a key role in physiological and pathological processes. Literature reports revealed that the conventional methods such as colorimetry, electron paramagnetic resonance (EPR), electrochemical <i>etc.</i> to detect NO are costly, time consuming and lack resolution, particularly in aqueous or biological system. Thus, in this context, herein we have developed covalently linked biomass derived carbon quantum dots (CQDs) and naphthalimide based nano sensor system for FRET based ratiometric detection of nitric oxide (NO) in pure aqueous media. The CQDs derived from orange peels were characterized using UV–visible absorption, fluorescence spectroscopy, PXRD, TEM, FT-IR and zeta potential studies. Further, the obtained CQDs were functionalized with amine functionality, and subsequently linked with naphthalimide derivative (<b>5</b>) using terephthaldehyde through covalent bond formation. The conjugation of naphthalimide (<b>5</b>) and functionalized CQDs was studied using DLS, zeta potential, FT-IR and time resolved fluorescence spectroscopy. The excitation of developed nano sensor system at <math>\lambda_{ex}</math> 360 nm results in fluorescence emission at <math>\lambda_{em}</math> 530 nm which establishes the FRET pair between the CQDs and naphthalimide unit. However, in the presence of NO, the observed FRET pair abolishes due to the cleavage of NO susceptible imine bond. The developed sensor demonstrates high selectivity towards NO with limit of detection (LOD) and limit of quantification (LOQ) of 15 nM and 50 nM respectively. Further, the developed sensor system was also utilized for indirect detection of nitrite (NO<sub>2</sub><sup>-</sup>) in food samples for food safety and monitoring.</p> <p><b>Graphical Abstract:</b></p>
22.	<p><a href="#">Fairness driven efficient algorithms for sequenced group trip planning query problem</a>  N Solanki, S Jain, S Banerjee, YP Kumar S - <i>Proceedings of the 2023 International Conference on Autonomous Agents and Multiagent Systems</i>, 2023</p>

	<p><b>Abstract:</b> The Group Trip Planning Query Problem (GTP) is a well-researched spatial database problem. Given a city road network with Point-of-Interests (PoIs) representing vertices divided into different categories, GTP aims to suggest one PoI from each category to minimize the group's total distance traveled. This paper focuses on sequenced GTP with pre-determined category visit order, studied under the constraints of fairness, and referred to as sequenced Fair Group Trip Planning Query Problem (Fair-GTP). While GTP aims to minimize the group's total travel time, Fair-GTP seeks to minimize the maximum time difference between any two agents in the group. Although solving group trip planning queries is NP-hard, we present polynomial time algorithms for finding optimal paths for both sequenced GTP and Fair-GTP. Our second significant result provides a bound on the price of fairness (PoF) representing the ratio of optimal path cost in sequenced Fair-GTP to optimal path cost in sequenced GTP. We show that while the PoF can go arbitrarily bad for general sequenced Fair-GTP solutions, restricting to Pareto-optimal solutions bounds the PoF by <math>(2b-1)</math>, where <math>b</math> denotes the number of agents traveling in the group. We further show that this bound is tight. Finally, we present the performance analysis of our algorithms on real-world datasets, demonstrating that our solution approach recommends PoIs within reasonable computational time, and in practice, PoF is below 2.</p>
23.	<p><a href="#">Fast response and high-performance UV-C to NIR broadband photodetector based on MoS<sub>2</sub>/a-Ga<sub>2</sub>O<sub>3</sub> heterostructures and impact of band-alignment and charge carrier dynamics</a>  R Wadhwa, D Kaur, Y Zhang, A Alexander, D Kumar...M Kumar - Applied Surface Science, 2023</p> <p><b>Abstract:</b> Recently, 2D materials have gained tremendous research interest due to their unique properties in electronics and optoelectronics. However, single 2D material-based photodetectors suffer from limitations such as narrow spectral sensitivity and slow response time due to bandgap restriction and difficulty in charge extraction. A heterojunction, which separates photo-excited electron-hole pairs and tunes absorption edge through appropriate selection of semiconductors with complementary bandgaps, is an effective strategy for broad spectral energy-conserving photodetection. This study presents a scalable 2D/3D heterostructure of MoS<sub>2</sub>/Ga<sub>2</sub>O<sub>3</sub> with outstanding UV-C to NIR broad spectral photoresponse. The MoS<sub>2</sub>/Ga<sub>2</sub>O<sub>3</sub> photodetector demonstrated a 315-fold increase in responsivity and EQE compared to pristine MoS<sub>2</sub> photodetector. The device showed highest responsivity and EQE of 171 AW<sup>-1</sup> and <math>2.4 \times 10^4</math> % respectively under 900 nm illumination at 5 V bias. The device also exhibits high detectivity (<math>4.6 \times 10^{13}</math> Jones) and fast response time of 97 <math>\mu</math>s. Moreover, the device is highly stable and shows no performance degradation over time. The device behavior was investigated through energy band diagrams and charge carrier dynamics using photoelectron spectroscopy and Kelvin probe force microscopy to gain intrinsic physical insights. The demonstration of MoS<sub>2</sub>/Ga<sub>2</sub>O<sub>3</sub> as a high-performance broadband photodetector offers exciting opportunities for efficient optoelectronics and imaging applications.</p> <p><b>Graphical abstract:</b> A 2D/3D heterostructure of MoS<sub>2</sub>/Ga<sub>2</sub>O<sub>3</sub> exhibits excellent performance in broadband photodetection, demonstrating an impressively wide photo-response range spanning from UV-C to NIR, with high responsivity and fast response time.</p> 
24.	<p><a href="#">Full cmos circuit for brain-inspired associative memory with on-chip trainable memristive stdp</a></p>

	<p><a href="#">synapse</a> SK Vohra, SA Thomas, M Sakare, DM Das - IEEE Transactions on Very Large Scale Integration (VLSI) Systems, 2023</p> <p><b>Abstract:</b> Spiking neural networks (SNNs) implemented in neuromorphic computing architectures promise a high degree of bio-plausibility and energy efficiency compared to the artificial neural network (ANN). Thus, SNN-based spiking associative memories are preferred for high capacity, area, and energy-efficient neural associative memories (NAMs). While most previously published works focused on ANN-based NAM, this work implements the full CMOS circuit of memristor crossbar-based spiking NAM for the first time. Instead of using any software-based memristive SPICE model or memristive devices that are yet not available in standard CMOS technology process design kits (PDKs), in our work, the CMOS-based memristive synapse circuit is employed to address practical circuit implementation challenges. The complete on-chip learning of the system is demonstrated using the bio-plausible spike-timing-dependent plasticity (STDP) learning mechanism without employing any external coprocessor, e.g., microprocessor, field-programmable gate array (FPGA). The entire system is implemented at the transistor level using 180-nm standard CMOS technology to demonstrate the pattern recognition application. The robustness of the proposed circuit is also evaluated to demonstrate the tolerance against the CMOS fabrication non-idealities.</p>
25.	<p><a href="#">Group fair clustering revisited -- notions and efficient algorithm</a> S Gupta, G Ghalme, NC Krishnan, S Jain - Proceedings of the 2023 International Conference on Autonomous Agents and Multiagent Systems, 2023</p> <p><b>Abstract:</b> This paper considers the problem of group fairness in clustering. We propose a new fairness notion which strictly generalizes existing notions, and we theoretically analyze the relationships between several existing notions. Finally, we propose a simple and efficient greedy round-robin-based algorithm (FRAC-OE) and extensive experiments to validate its efficacy across multiple datasets.</p>
26.	<p><a href="#">HFIP &amp; brønsted acid promoted direct distal c-alkylation of 2-oxindoles and anilines with donor-acceptor cyclopropanes</a> PR Singh, M Lamba, D Singh, A Goswami - Advanced Synthesis &amp; Catalysis, 2023</p> <p><b>Abstract:</b> Installation of an alkyl chain at a specified position in the aromatic ring <i>via</i> metal-free catalysis is very important. In this regard, we have developed a facile metal-free, extremely selective, user-friendly, environmentally benign and cost-effective Friedel-Crafts (FC) alkylation protocol for 2-oxindoles and anilines with donor-acceptor cyclopropanes. Real-time NMR studies reveal that the transformation is governed by the cooperative catalysis of Brønsted acid (TfOH) and HFIP, which facilitates the nucleophilic attack on donor-acceptor cyclopropanes from 2-oxindoles and anilines.</p> 
27.	<p><a href="#">Hydrogen storage in a ti-functionalized metal carbyne framework: insights from a first-principles study</a></p>

**Abstract:** Hydrogen ( $H_2$ ) has the ability to be a future green-energy source for the automotive industry due to its versatility, clean nature, and efficiency as an energy carrier. The biggest obstacle to achieving hydrogen as a potential energy source is the nonavailability of effective hydrogen storage materials. In this proposed work, the hydrogen storage capacity and reversibility of a Ti-functionalized metal carbyne framework (MCF) having carbyne as an organic linker and  $Mg_4O$  as an inorganic moiety are explored. All structural relaxation and simulation calculations are performed by employing the dispersion-corrected density functional theory computation. In this Ti-functionalized MCF, each Ti can adsorb up to five  $H_2$  molecules via the Kubas mechanism, with adsorption energy lying between 0.33 and 0.44 eV, which falls within the range outlined by the U.S. Department of Energy (DOE). For a detailed study of the thermal stability of framework, hydrogen reversibility, and mechanism of hydrogen sorption, Born–Oppenheimer molecular dynamics (BOMD) simulations are carried out at various temperatures. From the findings of BOMD simulations, the Ti-functionalized MCF can reversibly adsorb the  $H_2$  molecules with a high gravimetric density of about 9.4 wt %. This proposed Ti-functionalized MCF stands out as a potential hydrogen storage medium meeting the standards established by the DOE.



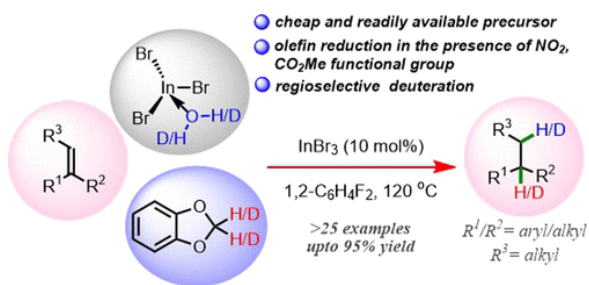
Identification of diphenylurea derivatives as novel endocytosis inhibitors that demonstrate broad-spectrum activity against SARS-CoV-2 and influenza A virus both in vitro and in vivo

N Kumar, IM Taily, C Singh, S Kumar, RS Rajmani..., P Singh...P Banerjee - PLoS pathogens, 2023

28.

**Abstract:** Rapid evolution of severe acute respiratory syndrome coronavirus 2 (SARS-CoV-2) and influenza A virus (IAV) poses enormous challenge in the development of broad-spectrum antivirals that are effective against the existing and emerging viral strains. Virus entry through endocytosis represents an attractive target for drug development, as inhibition of this early infection step should block downstream infection processes, and potentially inhibit viruses sharing the same entry route. In this study, we report the identification of 1,3-diphenylurea (DPU) derivatives (DPUDs) as a new class of endocytosis inhibitors, which broadly restricted entry and replication of several SARS-CoV-2 and IAV strains. Importantly, the DPUDs did not induce any significant cytotoxicity at concentrations effective against the viral infections. Examining the uptake of cargoes specific to different endocytic pathways, we found that DPUDs majorly affected clathrin-mediated endocytosis, which both SARS-CoV-2 and IAV utilize for cellular entry. In the DPUD-treated cells, although virus binding on the cell surface was unaffected, internalization of both the viruses was drastically reduced. Since compounds similar to the DPUDs were previously reported to transport anions including chloride ( $Cl^-$ ) across lipid membrane and since intracellular  $Cl^-$  concentration plays a critical role in regulating vesicular trafficking, we hypothesized that the observed defect in endocytosis by the DPUDs could be due to altered  $Cl^-$  gradient across the cell membrane. Using *in vitro* assays we demonstrated that the

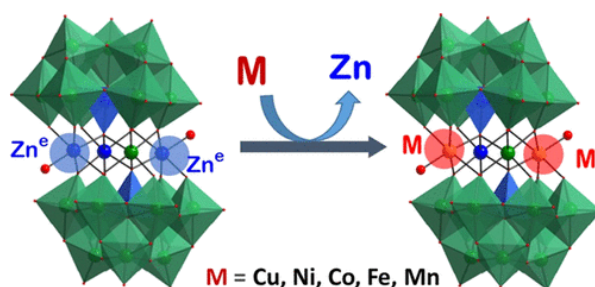


	<p>DPUDs transported <math>\text{Cl}^-</math> into the cell and led to intracellular <math>\text{Cl}^-</math> accumulation, which possibly affected the endocytic machinery by perturbing intracellular <math>\text{Cl}^-</math> homeostasis. Finally, we tested the DPUDs in mice challenged with IAV and mouse-adapted SARS-CoV-2 (MA 10). Treatment of the infected mice with the DPUDs led to remarkable body weight recovery, improved survival and significantly reduced lung viral load, highlighting their potential for development as broad-spectrum antivirals.</p>
29.	<p><a href="#">Identifying efficient policy mix under different targeting regimes: A tale of two crises</a>  SA Shah, B Garg - <i>Economic Analysis and Policy</i>, 2023</p> <p><b>Abstract:</b> We examine the influence of demand shock, supply shock and the monetary policy shock on macroeconomic variables using the New Keynesian Dynamic Stochastic General Equilibrium framework. Our study tries to identify the efficient monetary policy mix as an antidote to the prevailing economic fragilities that originated due to the COVID-19 pandemic and geopolitical conflict in case of India and China. Under both simulated and Bayesian analysis, our findings revealed the inflationary effect of demand and supply shock with a target-oriented monetary policy under sticky prices as the efficient policy tool to counter these effects. The macroeconomic projections depicted the favourable influence of output due to active intervention of target-oriented monetary policy in both these economies.</p>
30.	<p><a href="#">In-catalyzed transfer hydrogenation and regioselective hydrogen–deuterium addition to the olefins</a>  G Kumar, D Bhattacharya, P Mistry, I Chatterjee - <i>The Journal of Organic Chemistry</i>, 2023</p> <p><b>Abstract:</b> A unique and valuable methodology is developed for the hydrogenation of aromatic as well as aliphatic 1,1-di- and trisubstituted alkenes. In the presence of catalytic <math>\text{InBr}_3</math>, readily available 1,3-benzodioxole and residual <math>\text{H}_2\text{O}</math> present in the reaction mixture are utilized as a hydrogen gas surrogate and proved to be a practical source of deuterium incorporation into the olefins on either side by varying the source of the starting deuterated 1,3-benzodioxole or <math>\text{D}_2\text{O}</math>. Experimental studies show the transfer of hydride from 1,3-benzodioxole to the carbocationic intermediate generated from the protonation of alkenes by the <math>\text{H}_2\text{O}</math>–<math>\text{InBr}_3</math> adduct remains the critical step.</p>  <ul style="list-style-type: none"> <li>● cheap and readily available precursor</li> <li>● olefin reduction in the presence of <math>\text{NO}_2</math>, <math>\text{CO}_2\text{Me}</math> functional group</li> <li>● regioselective deuteration</li> </ul> <p><math>\text{InBr}_3</math> (10 mol%)  1,2-<math>\text{C}_6\text{H}_4\text{F}_2</math>, 120 °C  &gt;25 examples upto 95% yield  <math>\text{R}^1/\text{R}^2 = \text{aryl/alkyl}</math>  <math>\text{R}^3 = \text{alkyl}</math></p>
31.	<p><a href="#">Influence of build orientation on tensile and flexural strength of fdm fabricated abs component</a>  Anubhav, R Kumar, SK Nandi, A Agrawal - <i>Lecture Notes in Mechanical Engineering: Book Chapter</i>, 2023</p> <p><b>Abstract:</b> Additive manufacturing (AM) is a tool-free manufacturing process that has ability to fabricate a part with high dimensional accuracy with ease. Acrylonitrile butadiene styrene (ABS) is a commonly used 3D printing thermoplastic polymer with applications in various industries, viz., automotive and aerospace. Fused deposition modeling (FDM) is the most popular and extensively used extrusion-based AM technique to fabricate plastic parts, though the strength and anisotropic behavior of the fabricated part still require improvement. Part orientation during printing plays an important role in the printing process. In this work, a detailed analysis has been carried out on FDM-printed specimens of ABS material at different orientations ranging from 0</p>

	to 90° with vertical and horizontal. Tensile and flexural properties of ABS-printed specimens were evaluated to study the effect of build orientations and filament deposition in the FDM process. Fractography of fractured surfaces was also analyzed to study the fracture behavior of 3D-printed specimens.
32.	<p><a href="#">Low-intensity human activity recognition framework using audio data in an outdoor environment</a> P Choudhary, P Kumari, N Goel, M Saini - Communications in Computer and Information Science: Book Chapter, 2023</p> <p><b>Abstract:</b> Audio-based activity recognition is an essential task in a wide range of human-centric applications. However, most of the work predominantly focuses on event detection, machine sound classification, road surveillance, scene classification, etc. There has been negligible attention to the recognition of low-intensity human activities for outdoor scenarios. This paper proposes a deep learning-based framework for recognizing different low-intensity human activities in a sparsely populated outdoor environment using audio. The proposed framework classifies 2.0 s long audio recordings into one of nine different activity classes. A variety of audio sounds in an outdoor environment makes it challenging to distinguish human activities from other background sounds. The proposed framework is an end-to-end architecture that employs a combination of mel-frequency cepstral coefficients and a 2D convolutional neural network to obtain a deep representation of activities and classify them. The extensive experimental analysis demonstrates that the proposed framework outperforms existing frameworks by 16.43% on the parameter F1-score. Additionally, we collected and provided an audio dataset for evaluation and benchmarking purposes to the research community.</p>
33.	<p><a href="#">Measurement-based quantum Otto engine with a two-spin system coupled by anisotropic interaction: Enhanced efficiency at finite times</a> C Purkait, A Biswas - PHYSICAL REVIEW E, 2023</p> <p><b>Abstract:</b> We have studied the performance of a measurement-based quantum Otto engine (QOE) in a working system of two spins coupled by Heisenberg anisotropic interaction. A nonselective quantum measurement fuels the engine. We have calculated thermodynamic quantities of the cycle in terms of the transition probabilities between the instantaneous energy eigenstates, and also between the instantaneous energy eigenstates and the basis states of the measurement, when the unitary stages of the cycle operate for a finite time <math>\tau</math>. The efficiency attains a large value in the limit of <math>\tau \rightarrow 0</math> and then gradually reaches the adiabatic value in a long-time limit <math>\tau \rightarrow \infty</math>. For finite values of <math>\tau</math> and for anisotropic interaction, an oscillatory behavior of the efficiency of the engine is observed. This oscillation can be interpreted in terms of interference between the relevant transition amplitudes in the unitary stages of the engine cycle. Therefore, for a suitable choice of timing of the unitary processes in the short time regime, the engine can have a higher work output and less heat absorption, such that it works more efficiently than a quasistatic engine. In the case of an always-on heat bath, in a very short time, the bath has a negligible effect on its performance.</p>
34.	<p><a href="#">Near-infrared hyperspectral imaging in tandem with machine learning techniques to identify the near geographical origins of barley seeds</a> T Singh, A Sharma, NM Garg, SRS Iyengar - Lecture Notes in Networks and Systems, 2023</p> <p><b>Abstract:</b> The nondestructive identification of the geographical origins of the seeds is a crucial step in the food industry. The seeds from near geographical origins are challenging to be separated due to identical climatic and agronomic conditions. The current study implemented the idea of combining near-infrared hyperspectral imaging (NIR-HSI) with machine learning to distinguish barley seeds concerning their geographical origins. Hyperspectral images of barley seeds from four near geographical origins were captured within the range of 900–1700 nm. Sample-wise spectra were extracted from the hyperspectral images and pretreated with different spectral preprocessing techniques, viz., standard normal variate (SNV), multiplicative scatter</p>

	<p>correction (MSC), Savitzky–Golay smoothing (SGS), Savitzky–Golay first derivative (SG1), Savitzky–Golay second derivative (SG2), and detrending. Unprocessed and preprocessed sample-wise spectra were given as input to four different machine learning models. Support vector machines (SVMs), <i>K</i>-nearest neighbors (KNNs), random forest (RF), and partial least squares discriminant analysis (PLS-DA) were used for the classification based on the 1D spectral features. Among these classifiers, SVM showed the best classification accuracy of 93.66% when applied with the SG2 preprocessing technique. The results revealed the significance of using hyperspectral and machine learning to make a clear, fast, and accurate difference among barley varieties based on their geographical origins.</p>
35.	<p><a href="#">On subset selection of multiple humans to improve human-ai team accuracy</a>  S Singh, S Jain, SS Jha - <i>Proceedings of the 2023 International Conference on Autonomous Agents and Multiagent Systems</i>, 2023</p> <p><b>Abstract:</b> There are several classification tasks where neither the human nor the model is perfectly accurate. Some recent works, therefore, focus on the Human-AI team model, where the AI model's probabilistic output is combined with the human-predicted class label. The combined decision is shown to consistently outperform the model's or human's accuracy alone. All the previous works, however, restrict to the setting where they consider a single human to combine with the AI model. Motivated by the crowdsourcing literature, which combines labels from multiple humans, we show that combining multiple human labels with the model's probabilistic output can lead to significant improvement in accuracy. This paper further shows that while combining multiple humans helps, a naive combination of humans with AI model can lead to poor accuracy. Hence, there is a strong need for an intelligent strategy to select a subset of humans and combine their labels. To this end, we present an approach to merge the predicted labels from multiple humans with the model's probabilistic output. We then provide an efficient algorithm to find the optimal subset of humans whose combined labels offer the most accurate output. Finally, we empirically demonstrate that the combined model outperforms the AI model or any human alone in terms of accuracy. Besides this, our subset selection algorithm and combination method outperforms the single human model and other naïve combination techniques.</p>
36.	<p><a href="#">Pharmacological inhibition of DNMT1 restores macrophage autophagy and M2 polarization in Western diet-induced nonalcoholic fatty liver disease</a>  R Pant, SW Kabeer, S Sharma, V Kumar, D Patra, D Pal... - <i>Journal of Biological Chemistry</i>, 2023</p> <p><b>Abstract:</b> Nonalcoholic fatty liver disease (NAFLD) is associated with an increased ratio of classically activated M1 macrophages/Kupffer cells to alternatively activated M2 macrophages, which plays an imperative role in the development and progression of NAFLD. However, little is known about the precise mechanism behind macrophage polarization shift. Here, we provide evidence regarding the relationship between the polarization shift in Kupffer cells and autophagy resulting from lipid exposure. High-fat and high-fructose diet supplementation for 10 weeks significantly increased the abundance of Kupffer cells with an M1-predominant phenotype in mice. Interestingly, at the molecular level, we also observed a concomitant increase in expression of DNA methyltransferases DNMT1 and reduced autophagy in the NAFLD mice. We also observed hypermethylation at the promotor regions of autophagy genes (LC3B, ATG-5, and ATG-7). Furthermore, the pharmacological inhibition of DNMT1 by using DNA hypomethylating agents (azacitidine and zebularine) restored Kupffer cell autophagy, M1/M2 polarization, and therefore prevented the progression of NAFLD. We report the presence of a link between epigenetic regulation of autophagy gene and macrophage polarization switch. We provide the evidence that epigenetic modulators restore the lipid-induced imbalance in macrophage polarization, therefore preventing the development and progression of NAFLD.</p>
37.	<p><a href="#">Physico- and electrochemical properties of first-row transition-metal-substituted sandwich</a></p>

**Abstract:** The physico- and electrochemical behaviors of a series of  $[\text{WZn}_3(\text{H}_2\text{O})_2(\text{ZnW}_9\text{O}_{34})_2]^{12-}$  ( $\text{Zn-WZn}_3$ ) and its first-row transition-metal-substituted analogues  $[\text{WZn}(\text{TM})_2(\text{H}_2\text{O})_2(\text{ZnW}_9\text{O}_{34})_2]^{12-}$  ( $\text{Zn-WZn}(\text{TM})_2$ ;  $\text{TM} = \text{Mn}^{\text{II}}, \text{Co}^{\text{II}}, \text{Fe}^{\text{III}}, \text{Ni}^{\text{II}}$  and  $\text{Cu}^{\text{II}}$ ) are reported. Various spectroscopic studies, including Fourier transform infrared (FTIR) spectroscopy, UV-visible spectroscopy, electrospray ionization (ESI)-mass spectrometry, and Raman spectroscopy, show similar spectral patterns in all sandwich polyoxometalates (POMs) because of their isostructural geometry and constancy of the overall negative charge ( $-12$ ). However, the electronic properties highly depend on the transition metals at the “sandwich core” and correlate well with the density functional theory (DFT) study. Further, depending on the substituted TM atoms, there is a decrease in the highest occupied molecular orbital-lowest unoccupied molecular orbital (HOMO-LUMO) band-gap energy in these transition-metal-substituted POM (TMSP) complexes wrt  $\text{Zn-WZn}_3$ , as confirmed by diffuse reflectance spectroscopy and DFT study. Cyclic voltammetry reveals that the electrochemistry of these sandwich POMs ( $\text{Zn-WZn}_3$  and TMSPs) is highly dependent on the pH of the solution. Moreover, the dioxygen binding/activation studies of these polyoxometalates show that  $\text{Zn-WZn}_3$  and  $\text{Zn-WZnFe}_2$  have better efficiency toward dioxygen binding, as confirmed by FTIR spectroscopy, Raman spectroscopy, X-ray photoelectron spectroscopy (XPS), and thermogravimetric analysis (TGA), which is also reflected in their catalytic activity toward imine synthesis.



[Prediction of the future landslide susceptibility scenario based on LULC and climate projections](#)  
A Tyagi, RK Tiwari, N James - Landslides, 2023

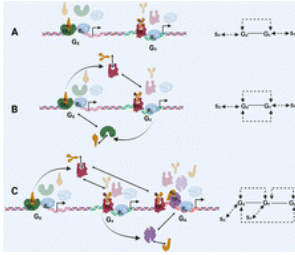
38.

**Abstract:** Worldwide, landslides are the most frequently occurring disaster that is very destructive and unpredictable in nature. A total of 850 landslide events were detected during 2005–2020 in the Tehri region of the Indian Himalayas. Many researchers have conducted landslide susceptibility mapping (LSM) studies for this region using different static landslide-causing factors. However, studies considering dynamic factors in predicting future landslide susceptibility scenarios are inadequate. Hence in this study, both dynamic and static factors were utilized in predicting future landslide susceptibility maps for the year 2050. The paper’s main objective is the future prediction of LSM, considering future projections of land use land cover (LULC) and climate variables (precipitation and temperature). To achieve this objective, first, the geospatial database in three temporal categories, 2005–2010, 2010–2015, and 2015–2020, was prepared for the historical landslide events. Second, the landslide-causing factors were optimized and utilized in LSM for 2010, 2015, and 2020. Third, projected LULC map was generated for the year 2050 using the Artificial Neural Network-Cellular Automata (ANN-CA) model. Fourth, CMIP6 climate projection maps were prepared using the Indian Institute of Tropical Meteorology Earth system model (IITM ESM) under four shared socioeconomic pathway (SSP) scenarios. Finally, the projected maps were used as the driving parameter for the future prediction of LSM. The results reveal a high increase in the built-up area (5%) and

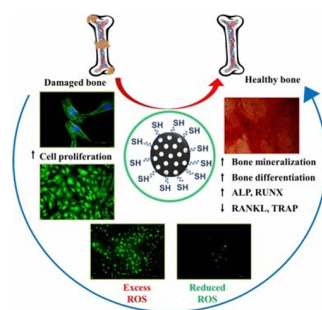


	<p>agriculture land (4%) with a decrease in forest area (10%) in future LULC projections. The results of future LSM prediction under SSP 1–2.6, SSP 2–4.5, SSP 3–7.0, and SSP 5–8.5 climate scenarios show an increase in very high landslide susceptibility class by 2%, 4%, 7%, and 9% respectively. The predicted maps were validated utilizing the Kappa coefficient verifies the reliability of the simulated future results.</p>
39.	<p><a href="#">Prioritization of sub-watersheds for the categorization of surface runoff and sediment production rate based on geo-spatial modeling and pca approach: a case from upper beas river, himachal pradesh, india</a>  M Kumar, RK Tiwari, K Kumar... - Journal of the Geological Society of India, 2023</p> <p><b>Abstract:</b> Studying geo-morphometric parameters using Remote Sensing (RS) and Geographic Information System (GIS) tools is crucial to routing runoff and remaining hydrological processes. A geo-spatial model and principal component analysis (PCA) approach are used in this study to prioritize sub-watersheds of the upper Beas river up to Pandoh dam. Dendritic drainage patterns throughout its sub-watersheds characterized the 6<sup>th</sup>-order Beas river. The sub-watersheds show a lithological uniformity that indicates that the entire watershed has structurally impermeable materials at both surface and sub-surface levels. Moreover, the aerial and relief aspects of the sub-watershed indicate fine drainage textures, steep slopes, immediate peak flows, a hydrograph with multiple peaks, and a low concentration time. In other words, the sub-watershed may not be able to manage flash floods during the storm period. Surface runoff and sediment production rates (SPR) were estimated in the present study ranged from 3.576–5.240 sq. km-cm/sq.km and 0.101–0.234 ha-m/100sq.km/year, respectively. Finally, the study concluded that the sub-watersheds in the upper regions produced high runoff and sediments, usually carried into the mainstream. Further, the PCA technique was applied to find the redundant morphometric parameters and then the same results were utilized to determine the effective way to prioritize the watershed. The present study will serve as a basis for developing appropriate policies and practices for peak flooding and promoting the sustainability of the watershed.</p>
40.	<p><a href="#">Scattering of water waves by two thin vertical barriers over shelf bottom topography</a>  N Kumar, A Kaur, SC Martha - Geophysical &amp; Astrophysical Fluid Dynamics, 2023</p> <p><b>Abstract:</b> In this paper, water waves interaction with two thin vertical barriers over shelf bottom topography is analysed using linearised wave theory. The associated mixed boundary value problem is solved with the aid of method involving eigenfunction expansions of the velocity potential and orthogonality relation of the eigenfunctions. Further, the resulting system of algebraic equations is solved using the least square method to find the physical quantities, that is, reflection and transmission coefficients, free surface elevation and non-dimensional horizontal force experienced by the barriers. The energy balance relation is derived from Green's identity which ensures the correctness of the present results. The obtained results are also compared with the results available in the literature for validation purpose. With the help of different plots, the effect of depth ratios, length of the barriers, angle of incidence and gap between the barriers is investigated for various values of physical parameters. The study reveals that the phenomena of zero reflection, that is, full transmission can be avoided by using non-identical barriers or asymmetric shelf bottom topography. Also, it is highlighted that the presence of two barriers instead of a single barrier over shelf topography will help to reduce the transmitted wave energy near the seashore. A generalisation of number of surface piercing barriers over the shelf bottom topography is also demonstrated.</p>
41.	<p><a href="#">Some factors of energy aid volatility across developing countries: A special focus on renewable sector</a>  P Jain, S Bardhan - Energy Policy, 2023</p> <p><b>Abstract:</b> Energy aid effectiveness is paramount for the timely achievement of Sustainable</p>

	<p>Development Goals (SDG)-7. However, the volatility of energy aid reduces its effectiveness. Given this, the paper empirically investigates the determinants of energy aid volatility and its renewable energy generation (REG) component for 76 aid-recipient countries during 2002–2019. By considering recipient and donor-specific factors, we also explore the linkages of all these factors with the direction of volatility, i.e., aid shortfalls and windfalls. Findings reveal that variations in energy/REG aid volatility reflect the recipient's macroeconomic and institutional characteristics more than donor-specific factors. Moreover, the impacts of all these factors vary across aid shortfalls and windfalls. Specifically, economic prosperity and aid dependency increase energy/REG aid volatility, infused by different directions of aid shocks. Contrarily, oil rents, political stability, and strong democracy reduce aid volatility. Multilateral donors provide more stable funding compared to bilateral donors. We also observe that donors provide stable REG aid in countries with inadequate renewable policies and clean development mechanism funding, playing a catalyst role in supporting institutionally weak countries in the renewable sector. We draw certain policy implications for donors and recipients to manage and mitigate the adverse consequences of volatile energy aid flows.</p>
42.	<p><a href="#">Statistical evaluation of snow accumulation and depletion from remotely sensed MODIS snow time series data using the SARIMA model</a>  M Kumar, RK Tiwari, K Kumar... - AQUA - Water Infrastructure, Ecosystems and Society, 2023</p> <p><b>Abstract:</b> In the remote and challenging terrain of the Himalayan region, accurate measurement of cyclic snow accumulation and depletion is a significant challenge. To overcome this, an attempt has been made in the present study by applying a statistical analysis of MODIS snow time series data with the Seasonal Autoregressive Integrated Moving Average (SARIMA) model from 2003 to 2018 over the Beas river basin. The Box–Jenkins methodology of forecasting is based on the identification using seasonality, stationarity, ACF, and PACF plots; and estimation based on maximum likelihood techniques; and the last diagnostic checking based on the residual and error values have been used. Later, forecasting models have been proposed separately for the snow accumulation period (October–February) as (1,1,1) (0,1,3)<sup>19</sup> and for the snow depletion period (March–September) as (1,1,1) (1,1,2)<sup>27</sup> after calibration of the data (2003–2015) and the same were then validated using data (2016–2018). The accuracy assessment of the models has been checked using performance criteria like AIC, MSE, and RSS. The comparison of the forecasting models with the observed data showed a good agreement with <math>R^2</math> of 0.83 and 0.89 for snow accumulation and snow depletion, respectively. This research highlights the potential of utilizing satellite data and statistical modeling to address the challenges of monitoring snow cover in remote and inaccessible regions.</p>
43.	<p><a href="#">Temporal variation of percolation and evapotranspiration components in the water cycle for the ropar district, punjab, india, using swat</a>  T Prashanth, S Ganguly - Lecture Notes in Civil Engineering: Book Chapter,2023</p> <p><b>Abstract:</b> Hydrological modeling is the mathematical representation of hydrological processes. Hydrological models analyze a basin's yield and response over time. Solving the continuity equation can quantify the amount of water available as direct surface runoff, groundwater recharge, evapotranspiration, etc., over time. It is observed that both annual/monthly precipitation and temperature vary with respect to time and space in the Ropar. The main objectives of this study are to validate the monthly average streamflow using the SWAT model at the Ropar headwork and determine the variation in groundwater recharge and evapotranspiration with respect to time at Ropar district in Punjab. The study also aims to analyze annual rainfall trends, evapotranspiration, and percolation obtained from SWAT from 2008 to 2019 at Ropar. The model was calibrated for the period from 2008 to 2015, and NSE of 0.55 was obtained in the study. The results are validated for the simulated flow for a period of 2016–2019 where <math>R^2</math> value of 0.722 and NSE value of 0.6 are achieved.</p>

44.	<p><a href="#">The impact of light polarization and the nature of modes in the formation of quasi-bound states in the continuum at near-normal incidence</a>  Satwik PNV, M Khokhar, RV Nair - Journal of Physics D: Applied Physics, 2023</p> <p><b>Abstract:</b> Bound states in the continuum (BIC) is a peculiar resonant mode with an infinite radiative lifetime and quality factor (<math>Q</math>-factor) embedded within the radiation continuum, which find applications in sensing, lasing, and quantum photonics. While an ideal BIC with an infinite <math>Q</math>-factor can only occur in theory, observing quasi-BIC in realistic samples with finite sizes is possible. However, the robustness of quasi-BIC depends primarily on the trapped electromagnetic modes. Here, we discuss the polarization dependence and the nature of quasi-BIC mode in a two-dimensional array of gallium arsenide (GaAs) scatterers through finite difference time domain simulations and analytical calculations. The calculated angle- and polarization-dependent transmission spectra show quasi-BIC evolution with high <math>Q</math>-factor at near-normal incidence only for transverse magnetic polarization. The calculated total scattering cross-section implies the dominant contribution from electric dipole moments in generating the quasi-BIC. The evolution of quasi-BIC mode is discussed in terms of Mie or Fabry–Perot modes using geometry-dependent transmission and field intensity calculations. The proposed GaAs metasurfaces with quasi-BIC at 638 nm, corresponding to the zero phonon line of nitrogen-vacancy centers in diamond are useful for applications in photonic quantum technologies.</p>
45.	<p><a href="#">Theoretical investigation of functional responses of bio-molecular assembly networks</a>  P Gautam, SK Sinha – Soft Matter, 2023</p> <p><b>Abstract:</b> Cooperative protein–protein and protein–DNA interactions form programmable complex assemblies, often performing non-linear gene regulatory operations involved in signal transductions and cell fate determination. The apparent structure of those complex assemblies is very similar, but their functional response strongly depends on the topology of the protein–DNA interaction networks. Here, we demonstrate how the coordinated self-assembly creates gene regulatory network motifs that corroborate the existence of a precise functional response at the molecular level using thermodynamic and dynamic analyses. Our theoretical and Monte Carlo simulations show that a complex network of interactions can form a decision-making loop, such as feedback and feed-forward circuits, only by a few molecular mechanisms. We characterize each possible network of interactions by systematic variations of free energy parameters associated with the binding among biomolecules and DNA looping. We also find that the higher-order networks exhibit alternative steady states from the stochastic dynamics of each network. We capture this signature by calculating stochastic potentials and attributing their multi-stability features. We validate our findings against the Gal promoter system in yeast cells. Overall, we show that the network topology is vital in phenotype diversity in regulatory circuits.</p> 
46.	<p><a href="#">Thiol-functionalized, antioxidant, and osteogenic mesoporous silica nanoparticles for osteoporosis</a>  N Rasool, D Negi, Y Singh - ACS Biomaterials Science &amp; Engineering, 2023</p> <p><b>Abstract:</b> Osteoporosis is a chronic bone disorder characterized by decreased bone mass, leading to brittle bones and fractures. Oxidative stress has been identified as the most profound</p>

trigger for the initiation and progression of osteoporosis. Current treatment strategies do not induce new bone formation and fail to address a high level of reactive oxygen species (ROS). Mesoporous silica nanoparticles (MSNs) have been explored in bone tissue regeneration owing to their inherent osteogenic property, but they lack antioxidant and cell adhesion properties, required in such applications. We have developed thiolated, bioactive mesoporous silica nanoparticles (MSN-SH) to address this challenge. MSNs were fabricated using the Stöber method, and 11% of the surface was functionalized post-synthesis with thiol groups using MPTMS to obtain MSN-SH. The particle size measured by the dynamic light scattering technique was found to be around 300 nm. The surface morphology was investigated using HR-TEM, and their physical and chemical properties were characterized using various spectroscopic techniques. They exhibited more than 90% antioxidant activity, neutralized ROS formed in cells, and provided protection against ROS-induced cell damage. The cell viability assay in murine osteoblast precursor cells (MC3T3) showed that MSN-SH is cell-proliferative in nature with 140% cell viability. Osteogenic potential was evaluated by measuring the ALP activities, calcium deposition, and gene expression levels of osteogenic markers, such as RUNX2, ALP, OCN, and OPN, and results revealed that MSN-SH increases calcium deposition and induces osteogenesis through upregulation of osteogenic genes and markers without the involvement of any osteogenic supplements. Besides promoting osteogenesis, MSN-SH was found to inhibit osteoclastogenesis. The nanomaterial was found to be regenerative in nature, and it stimulated migration of osteoblast cells and caused a complete wound closure within 48 h. We were able to achieve a multifunctional nanomaterial by simply modifying the surface. MSNs have been explored for bone tissue engineering/osteoporosis as a composite system incorporating metals, like gold and cerium, or as a nanocarrier loaded with growth factors or active drugs. This study offers a simple and economical method to enhance the existing properties of MSNs and impart new activities by a single-step surface modification. It can be concluded that MSN-SH holds promise as a complementary and alternate treatment for osteoporosis along with the standardized therapy.



[Three-dimensional spheroid culture of dental pulp-derived stromal cells enhance their biological and regenerative properties for potential therapeutic applications](#)

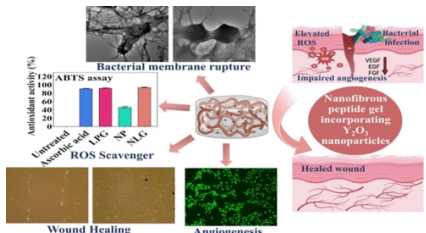
S Raik, P Sharma, S Kumar, V Rattan...N Kumar... - The International Journal of Biochemistry & Cell Biology, 2023

47.

**Abstract:** Mesenchymal stem/stromal cell (MSC) spheroids generated in a three-dimensional (3D) culture system serve as a surrogate model that maintain stem cell characteristics since these mimic the *in vivo* behavior of cells and tissue more closely. Our study involved a detailed characterization of the spheroids generated in ultra-low attachment flasks. The spheroids were evaluated and compared for their morphology, structural integrity, viability, proliferation, biocomponents, stem cell phenotype and differentiation abilities with monolayer culture derived cells (2D culture). The in-vivo therapeutic efficacy of DPSCs derived from 2D and 3D culture was also assessed by transplanting them in an animal model of the critical-sized calvarial defect. DPSCs formed compact and well-organized multicellular spheroids when cultured in ultra-low



	<p>attachment condition with superior stemness, differentiation, and regenerative abilities than monolayer cells. They maintained lower proliferative state and showed marked difference in the cellular biocomponents such as lipid, amide and nucleic acid between DPSCs from 2D and 3D cultures. The scaffold-free 3D culture efficiently preserves DPSCs intrinsic properties and functionality by maintaining them in the state close to the native tissues. The scaffold free 3D culture methods allow easy collection of a large number of multicellular spheroids of DPSCs and therefore, this can be adopted as a feasible and efficient method of generating robust spheroids for various in-vitro and in-vivo therapeutic applications.</p>
48.	<p><a href="#">Tunable Regio- and Stereoselective Synthesis of Z-Acrylonitrile Indoles and 3-Cyanoquinolines from 2-Alkynylanilines and Alkynyl nitriles</a> M Kumar, A Goswami - Organic Letters, 2023</p> <p><b>Abstract:</b> The merger of two bifunctional moieties, 2-alkynylaniline and alkynyl nitriles, in the presence of ZnBr<sub>2</sub> offers the tunable synthesis of two biologically important motifs: acrylonitrile indoles and 3-cyanoquinolines. The group present on the terminal alkyne of 2-alkynylaniline regulates the reaction pathways, intra- versus intermolecular, which thereby adds stereoselectivity and regioselectivity in this protocol. The conversion of an acrylonitrile indole ring to quinoline is an intriguing synthetic utility of this methodology.</p>
49.	<p><a href="#">Voltage support and imbalance mitigation during voltage sags by renewable energy fed grid connected inverters</a> AH Lone, AI Gedam, RK Sekhar – IEEE IAS Global Conference on Renewable Energy and Hydrogen Technologies, 2023</p> <p><b>Abstract:</b> In this study, symmetrical component-based current injection is used to analyse a single-stage grid-connected inverter with low voltage ride-through (LVRT) capability. During voltage sags, the renewable source-fed voltage source inverter (VSI) may disconnect from the main grid at the point of common coupling. This condition arises due to the Under-voltage/over-current protection in the renewable inverters. This sudden dis-connecting of the inverters may cause voltage collapse, frequency instability, and synchronous angle instability in utility networks with significant penetration of power from renewable inverters, which can result in blackouts. Utility grid rules require low-voltage ride-through capabilities in grid-connected inverters to mitigate this effect. In order to support voltage and reduce volt-age imbalance at the point of common coupling, a symmetrical component-based real and reactive power injection approach has been developed in this study. This technique is implemented by considering the constraint of not exceeding the inverter's rated current capability. The proposed technique effectively boosted the positive sequence voltage component to a reference value by using a PI controller. The negative sequence reactive power was drawn using the remaining reactive power capacity in order to suppress the voltage's negative sequence component. Results are presented in the paper for various voltage sag conditions. The proposed techniques are validated by simulating the model in a Matlab simulink environment.</p>
50.	<p><a href="#">Water security and health risk assessment of an urban household-level drinking water and sanitation system, Punjab, India</a> M Verma, VA Loganathan - Environmental Monitoring and Assessment, 2023</p> <p><b>Abstract:</b> The water scarcity and deteriorating water quality are major issues of concern to the agrarian state of Punjab, India. The focus of the study is to assess the status of drinking water and sanitation systems of Punjab using an exhaustive dataset of 1575 drinking water samples from 433 sampling locations in 63 urban local bodies of Punjab. Water security index (WSI) indicate that out of 63 urban local bodies, 13 are categorized into good class, 31 fall under fair class, and 19 fall under poor class. The access indicator under sanitation dimension shows that Bathinda region has maximum sewerage network coverage relative to other regions, whereas ca. 50% of the ULBs in Amritsar region do not have sewerage facility. It is clearly depicted that the</p>

	<p>variation in WSI is mainly attributable to sanitation dimension (10–22.5) as variation in water supply dimension (29–35) is relatively less. Hence, emphasis on indicators and variables of sanitation dimension is required for the improvement of overall WSI. The assessment of qualitative aspects of drinking water and health risk depicts that the drinking water quality of southwest part of the state (i.e. Malwa region) is under good quality class contrary to its poor groundwater quality. Kapurthala district shows high health risk due to the presence of trace metals despite being classified into good class within water security index. The drinking water quality is better and health risks are minimal in regions where drinking water is supplied via treated surface water sources (e.g. Bathinda region). Furthermore, the results of health risk assessment correlate with M<sub>ED</sub>-Water Quality Index outcome owing to presence of trace metals in groundwater above permissible limits. These results will help in identification of shortcomings in water supply and sanitation infrastructure and its management in urban areas.</p>
51.	<p><a href="#">Yttrium oxide nanoparticle-loaded, self-assembled peptide gel with antibacterial, anti-inflammatory, and proangiogenic properties for wound healing</a>  V Chawla, S Sharma, Y Singh - ACS Biomaterials Science &amp; Engineering, 2023</p> <p><b>Abstract:</b> Chronic wounds are a major healthcare challenge owing to their complex healing mechanism and number of impediments to the healing process, like infections, unregulated inflammation, impaired cellular functions, poor angiogenesis, and enhanced protease activity. Current topical care strategies, such as surgical debridement, absorption of exudates, drug-loaded hydrogels for infection and inflammation management, and exogenous supply of growth factors for angiogenesis and cell proliferation, slow the progression of wounds and reduce patient suffering but suffer from low overall cure rates. Therefore, we have developed a proteolytically stable, multifunctional nanoparticle loaded-peptide gel with inherent anti-inflammatory, antibacterial, and pro-angiogenic properties to provide a favorable wound healing milieu by restoring impaired cellular functions. We have fabricated a self-assembled, lauric acid-peptide conjugate gel, LA-<sup>L</sup>Lys-<sup>D</sup>Phe-<sup>L</sup>Lys-NH<sub>2</sub>, loaded with yttrium oxide (Y<sub>2</sub>O<sub>3</sub>) nanoparticles (NLG). Gel formed a nanofibrous structure, and nanoparticles were passively entrapped within the network. The surface morphology, stability, viscoelastic, and self-healing characteristics of gels were characterized. It showed a high stability against degradation by proteolytic enzymes and highly potent antibacterial activities against <i>E. coli</i> and <i>S. aureus</i> due to the presence of positively charged side chains of lysine in the peptide chain. It also exhibited an excellent antioxidant activity as well as ability to stimulate cell proliferation in murine fibroblast (L929) cells and human umbilical vein endothelial cells (HUVECs). The incorporation of nanoparticles promoted angiogenesis by upregulating pro-angiogenic genes, vascular endothelial growth factor (VEGF), fibroblast growth factor (FGF2), and epidermal growth factor (EGFR), and the gel caused complete wound closure in cells. In summary, the Y<sub>2</sub>O<sub>3</sub> nanoparticle-loaded lauric acid-peptide conjugate gel is able to elicit the desired tissue regeneration responses and, therefore, has a strong potential as a matrix for the treatment of chronic wounds.</p>  <p>The figure illustrates the multifunctional properties of the Yttrium oxide nanoparticle-loaded peptide gel. It includes a bar chart showing ROS scavenger activity for various samples (Lauric acid, NLG, LA-NLG, Lys, Phe, and Me), a diagram of bacterial membrane rupture, a schematic of a nanofibrous peptide gel incorporating Y<sub>2</sub>O<sub>3</sub> nanoparticles, and images of wound healing and angiogenesis.</p>